Extension of scaled particle theory to inhomogeneous hard particle fluids. II. Theory and simulation of fluid structure surrounding a cavity that intersects a hard wall

Daniel W. Siderius and David S. Corti*
School of Chemical Engineering, Purdue University, 480 Stadium Mall Drive, West Lafayette, Indiana 47907-2100, USA
(Received 23 November 2004; published 25 March 2005)

Integral equations describing the structure of a hard sphere fluid surrounding a cavity that intersects a hard wall are derived from scaled particle theory (SPT). The new expressions are solved exactly for specific cavity radii and the predictions are compared to simulation-generated results, showing excellent agreement. Additional simulation studies are conducted for cavity radii that fall outside the range of exact solution. For all cavity sizes, an enhancement of the local density of hard spheres over that of the hard wall contact value is seen for positions near the point of intersection of the cavity and the hard wall. The local density in front of the cavity and away from the hard wall is depleted at small cavity sizes, but eventually approaches the density profile created by a cavity placed within a bulk hard sphere fluid at larger cavity radii. The exact solutions and simulation results are also used to understand why a minimum appears in the inhomogeneous SPT function $\overline{G}(\lambda,h)$ [D. W. Siderius and D. S. Corti, preceding paper, Phys. Rev. E **71**, 036141 (2005)].

DOI: 10.1103/PhysRevE.71.036142 PACS number(s): 05.20.−y, 61.20.−p, 68.03.−g, 82.70.Dd

I. INTRODUCTION

In our preceding paper [1], the equations of scaled particle theory (SPT) [2] were extended to a hard sphere fluid confined by planar hard walls. A new function, $\overline{G}(\lambda,h)$, was introduced to describe the average density of particle centers contacting the surface of a cavity that intersected a hard wall in which the cavity center was located a distance h from a chosen reference plane. This function was determined exactly for various radii, similar to its bulk analog, and was interpolated beyond the exact limit using an asymptotic series. $\overline{G}(\lambda,h)$ was then used to describe the average pressure exerted on the cavity surface or, more importantly, to calculate the reversible work of cavity insertion. The work predictions agreed quite well with simulation results.

The function $\overline{G}(\lambda,h)$ is related to the the key quantity of any version of SPT, $G(\lambda,\theta,h)$, where $\rho G(\lambda,\theta,h)$ is defined as the local density of hard sphere centers at an angle θ in contact with the surface of a cavity of radius λ centered at $z=h\leqslant 0$, and ρ is the density of particle centers in the bulk phase (see Fig. 3 for the definition of the chosen coordinate system). For a review of both traditional SPT [2,3] and the development of inhomogeneous SPT, the reader is referred to our companion paper [1]. In traditional SPT, where cavities are inserted into a bulk uniform fluid, G is not a function of θ or h because the system is isotropic. Within inhomogeneous SPT (or I-SPT) this dependence cannot be overlooked since the fluid is anisotropic near the hard wall. Consequently, the average function, $\overline{G}(\lambda,h)$, exhibits behavior markedly different from the bulk $G(\lambda)$. Whereas $G(\lambda)$ begins at unity (for $\lambda=0$) and asymptotically approaches $p/\rho kT$ as $\lambda\to\infty$, $\overline{G}(\lambda,h)$ begins at the value of $p/\rho kT$ (for $\lambda=-h$), initially decreases for larger λ, only to return to its final value of $p/\rho kT$ as $\lambda\to\infty$. This behavior was attributed to the influence of the fluid structure, and thereby the line tension, that develops around the cavity that intersects the hard wall. Yet, the development of I-SPT in Ref. [1] could not provide any information about the exact geometric origin of this behavior. A more detailed explanation of the properties of $\overline{G}(\lambda,h)$ is the main purpose of this paper.

As shown in Ref. [1], $G(\lambda,\theta,h)$ may be averaged over the valid θ-range to produce the average SPT function $\overline{G}(\lambda,h)$. This average function is defined by

$$\overline{G}(\lambda,h)=\frac{2\pi\int_0^{\cos^{-1}(-h/\lambda)}G(\lambda,\theta,h)\sin\theta d\theta}{2\pi\int_0^{\cos^{-1}(-h/\lambda)}\sin\theta d\theta}. \tag{1}$$

A number of formally *exact* expressions can be obtained for $\overline{G}(\lambda,h)$. For example, the probability of observing a cavity of radius of at least λ centered at $z=h$ relative to the wall, $P_0(\lambda,h)$, is related to $\overline{G}(\lambda,h)$ via

$$\rho\overline{G}(\lambda,h)=\frac{-1}{2\pi(\lambda^2+\lambda h)}\frac{\partial\ln P_0(\lambda,h)}{\partial\lambda}. \tag{2}$$

For $\lambda\leqslant\sqrt{h^2+(\sigma/2)^2}$, $P_0(\lambda,h)$ is known exactly in which

$$P_0(\lambda,h)=1-\pi\int_0^{\lambda+h}\rho(z)[\lambda^2-(z-h)^2]dz,$$

$$\lambda\leqslant\sqrt{h^2+\left(\frac{\sigma}{2}\right)^2}, \tag{3}$$

where $\rho(z)$ is the local density of hard spheres at a distance z from the hard wall when no cavity is present. Substitution of

*Electronic address: dscorti@ecn.purdue.edu

the above into Eq. (2) yields the following exact form of $\overline{G}(\lambda,h)$:

$$\rho\overline{G}(\lambda,h)=\frac{\int_0^{\lambda+h}\rho(z)dz}{(\lambda+h)\left(1-\pi\int_0^{\lambda+h}\rho(z)[\lambda^2-(z-h)^2]dz\right)},$$

$$\lambda\leqslant\sqrt{h^2+\left(\frac{\sigma}{2}\right)^2}. \tag{4}$$

Integration of Eq. (2) also reveals that

$$P_0(\lambda,h)=\exp\left(-2\pi\rho\int_{-h}^{\lambda}\overline{G}(r,h)(r^2+rh)dr\right). \tag{5}$$

These four exact relations will prove useful in later sections of this paper.

Although averaging $G(\lambda,\theta,h)$ over the surface of the cavity to produce $\overline{G}(\lambda,h)$ assists in the derivation of useful physical and statistical mechanical quantities, more detailed information regarding the fluid structure about the cavity, i.e., information on $G(\lambda,\theta,h)$, is unfortunately lost. A better understanding of $G(\lambda,\theta,h)$ is, for example, important for a complete description of the depletion, or entropic, forces that arise between a hard particle and a hard wall. The true origin of depletion forces in hard particle systems resides in the geometric distribution of solvent particle centers surrounding the solute or the equivalent cavity [4]. Additional knowledge of the θ dependence of $G(\lambda,\theta,h)$ will therefore lead to a better understanding of the geometric effects that yield both attractive and repulsive depletion phenomena.

In what follows, we present the derivation of an integral equation that describes the fluid structure surrounding a cavity that intersects a hard wall. Using this equation, we obtain for certain cavity radii the exact form of $G(\lambda,\theta,h)$. This integral equation is based on the SPT integral equation first derived by Reiss and Casberg [5] to approximate the radial distribution function of the hard sphere fluid. Lee [6] later derived the same equation, though starting from a set of relations provided by Reiss *et al.* [7]. Here, we extend the approach of Refs. [6,7] to describe cavities intersecting a hard wall and, when possible, solve the resultant equation exactly. We also present simulation data at cavity sizes for which the integral equation cannot be solved exactly. Overall, the integral equation provides the needed information to understand why the I-SPT function $\overline{G}(\lambda,h)$ exhibits a minimum [1], despite the appearance of a density enhancement at the point of intersection between the cavity and the hard wall.

The paper is organized as follows. Section II reviews the derivation of the bulk SPT integral equation. Section III includes a definition of the current system geometry and contains a complete derivation of the SPT integral equation now applicable to cavities located at a hard wall. An exact closure condition is also presented. Section IV discusses the numerical results obtained from the solution of the integral equation for hemispherical cavities ($h=0$) in the exact range and simulation data for those outside the exact range. The paper is concluded in Section V.

II. REVIEW OF THE SPT INTEGRAL EQUATION FOR THE BULK HARD SPHERE FLUID

Before discussing the extension of the SPT integral equation to inhomogeneous fluids, we provide a somewhat detailed overview of the integral equation that is applicable to unconfined, isotropic hard sphere fluids. This integral equation was first derived by Reiss and Casberg [5], though the derivation given below follows from a similar analysis developed later by Reiss *et al.* [7].

We begin with the definition of an auxiliary function. Consider some arbitrary point within the fluid and suppose that a cavity of radius of at least λ is centered at that point. Let $\beta(\lambda,\mathbf{R})d\mathbf{R}$ represent the probability of observing the near particle center (i.e., nearest neighbor) to the cavity at $\mathbf{R}$ in $d\mathbf{R}$, where $\mathbf{R}$ is the vector joining the cavity center (chosen to be the origin) and the hard particle center. There is no angular dependence in an isotropic fluid, thus $\beta(\lambda,\mathbf{R})=\beta(\lambda,R)$, where $R\equiv|\mathbf{R}|$. Later, we will see that this symmetry does not exist for fluids confined between hard walls. This nearest neighbor probability is related to two other statistical geometric quantities through [7]

$$\beta(\lambda,R)d\mathbf{R}=P_0(R|\lambda)\rho G(R)d\mathbf{R}. \tag{6}$$

The first term on the right side, $P_0(R|\lambda)$, is the probability of observing a cavity of radius of at least R on the condition that a cavity of radius λ is present at the origin. $P_0(R|\lambda)$ is then multiplied by the probability of observing a particle at $\mathbf{R}$ in $d\mathbf{R}$, or $\rho G(R)d\mathbf{R}$, where $\rho G(R)$ is the local density of particle centers contacting a cavity of radius R, to give the probability of finding the nearest neighbor at $\mathbf{R}$ in $d\mathbf{R}$. By argument of conditional probabilities one can write [2]

$$P_0(R|\lambda)=\frac{P_0(R)}{P_0(\lambda)}=\exp\left(-4\pi\rho\int_\lambda^R G(r)r^2dr\right), \tag{7}$$

where the exponential term results from substitution of the SPT form for P_0 similar to Eq. (5). Therefore,

$$\beta(\lambda,R)=\rho G(R)\exp\left(-4\pi\rho\int_\lambda^R G(r)r^2dr\right). \tag{8}$$

Where $R=\lambda$, we have that

$$\beta(\lambda,\lambda)=\rho G(\lambda). \tag{9}$$

Also, a derivative of Eq. (8) that will later prove useful is [7]

$$\frac{\partial\beta(\lambda,R)}{\partial\lambda}=\rho G(R)\exp\left(-4\pi\rho\int_\lambda^R G(r)r^2dr\right)[4\pi\rho G(\lambda)\lambda^2]$$
$$=4\pi\rho G(\lambda)\lambda^2\beta(\lambda,R). \tag{10}$$

A. Derivation of the bulk SPT integral equation

Now consider the cavity-particle correlation function $\rho g(\lambda,\mathbf{R})d\mathbf{R}$, which denotes the probability of finding a par-

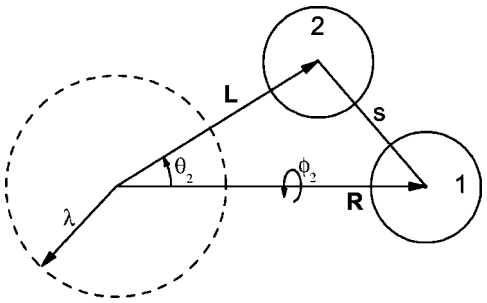

FIG. 1. Diagram of a given configuration of two hard spheres near a spherical cavity of radius λ. The dashed line represents the cavity in which its nearest neighbor is at position **L** and is labeled particle 2. The particle at **R** is labeled 1. s is the distance between the two hard particle centers. θ_2 measures the angle between **R** and **L**, while ϕ_2 measures the rotation around **R**.

ticle center at **R** in $d\mathbf{R}$ given that a cavity of radius λ is located at the origin. Isotropy again demands that $g(\lambda,\mathbf{R})=g(\lambda,R)$. Since a cavity of radius of $\lambda=\sigma$ is also equivalent to another hard particle [2], $g(\sigma,R)$ is identical to $g(R)$, the radial distribution function of the pure component hard sphere fluid. The cavity-particle correlation function can be represented by the following formally exact integral equation [7],

$$\rho g(\lambda,R)d\mathbf{R}=\beta(\lambda,R)d\mathbf{R}+\left(\int_{|\mathbf{L}|=\lambda}^{|\mathbf{L}|=R}\beta(\lambda,L)\rho g^{[3]}(\mathbf{L},\mathbf{R})d\mathbf{L}\right)d\mathbf{R}. \tag{11}$$

The origin of the two terms in Eq. (11) is illustrated in Fig. 1. Let the particle whose center is found at **R** in $d\mathbf{R}$ be labeled 1. Now, particle 1 may be the nearest neighbor to the cavity, hence giving rise to the first term on the right-hand side of Eq. (11). If particle 1 is not the nearest neighbor, then another particle, say 2, is the nearest neighbor and is located at **L** in $d\mathbf{L}$. (Clearly, $\lambda\leqslant L\leqslant R$, where $L\equiv|\mathbf{L}|$.) The second term on the right-hand side of Eq. (11) results from multiplying $\beta(\lambda,L)d\mathbf{L}$, the probability that the nearest neighbor, particle 2, is at **L** in $d\mathbf{L}$, by $\rho g^{[3]}(\mathbf{L},\mathbf{R})d\mathbf{R}$, the probability of observing particle 1 at **R** in $d\mathbf{R}$ given a cavity of radius λ at the origin and the nearest neighbor 2 at **L** in $d\mathbf{L}$. The resulting total probability is then integrated over all positions in which particle 2 is the nearest neighbor. Because the fluid is isotropic, $g^{[3]}$ only depends on R and not the vector position **R**. Hence, $g^{[3]}(\mathbf{L},\mathbf{R})=g^{[3]}(\mathbf{L},R)$.

Equation (11), which describes the fluid structure surrounding a cavity, is formally *exact* but cannot be used to solve for $g(\lambda,R)$ without knowledge of $g^{[3]}(\mathbf{L},R)$. $g^{[3]}$ is not known in general, however, and an approximate form, or closure condition, must be introduced into Eq. (11). This SPT integral equation is fundamentally different from previous integral equations in that the definition of the three-body correlation $g^{[3]}$ is not tied to Eq. (11). In fact, $g^{[3]}$ can be computed directly from simulation [6,8] without the use of Eq. (11). Consequently, the generation of closure conditions for $g^{[3]}$ can rely heavily upon physical intuition.

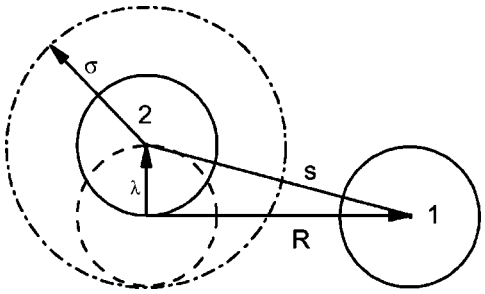

FIG. 2. A particular configuration of two hard spheres that is described by the correlation function $g^{[3]}(\lambda,\theta_2,R)$ in which $\lambda\leqslant\sigma/2$. The cavity of radius λ is denoted by the dashed line and the center of particle 2 is found on the cavity surface. The exclusion sphere of particle 2 is given by the dashed-dot line, denoting the region in which no other particle center may be found. Particle 1 is located a distance of R from the cavity center and its distance to particle 2 is s.

For later use, manipulation of Eq. (11) simplifies the introduction of a closure condition for $g^{[3]}$ that allows for an exact solution of the SPT integral equation for a limited range of λ and R. Differentiating Eq. (11) with respect to λ, using Leibnitz's rule, yields the following derivative of $g(\lambda,R)$ [5],

$$\begin{aligned}\rho\frac{\partial g(\lambda,R)}{\partial\lambda}=\frac{\partial\beta(\lambda,R)}{\partial\lambda}-\rho\Bigg(&\beta(\lambda,\lambda)\int_0^\pi\sin\theta_2 d\theta_2\\&\times\int_0^{2\pi}d\phi_2 g^{[3]}(\lambda,\theta_2,\phi_2,R)\\&-\int_\lambda^R L^2dL\frac{\partial\beta(\lambda,L)}{\partial\lambda}\int_0^\pi\sin\theta_2 d\theta_2\\&\times\int_0^{2\pi}d\phi_2 g^{[3]}(L,\theta_2,\phi_2,R)\Bigg),\end{aligned} \tag{12}$$

where we have used (L,θ_2,ϕ_2) as the coordinates for particle 2 and expanded $d\mathbf{L}$ to $L^2\sin\theta_2 d\theta_2 d\phi_2$. Because the system is isotropic, there is no ϕ_2 dependence. Thus, substitution of Eqs. (9) and (10) into Eq. (12) and integration over the ϕ_2 terms reduces the above to [5]

$$\begin{aligned}\frac{\partial g(\lambda,R)}{\partial\lambda}=&4\pi\rho\lambda^2G(\lambda)g(\lambda,R)\\&-2\pi\rho\lambda^2G(\lambda)\int_0^\pi\sin\theta_2 d\theta_2 g^{[3]}(\lambda,\theta_2,R).\end{aligned} \tag{13}$$

Equation (13) provides a more convenient starting point than Eq. (11) for obtaining $g(\lambda,R)$ when an expression for $g^{[3]}(\lambda,\theta_2,R)$ is generated. In Eq. (13), one can see that $g^{[3]}$ is evaluated for $L=\lambda$, meaning particle 2 always resides on the surface of the cavity (see Fig. 2). This greatly simplifies further analysis, since we only need to consider configurations where particle 2 is on the cavity surface when determining an expression for $g^{[3]}$.

B. Exact analysis of $g^{[3]}(\lambda,\theta_2,R)$ for $\lambda \leqslant \sigma/2$

Because $L=\lambda$ in $g^{[3]}$, the only configurations that need to be considered are similar to the one displayed in Fig. 2, in which the center of particle 2 is located on the cavity surface. Furthermore, as illustrated in Fig. 2, when $\lambda \leqslant \sigma/2$, the exclusion sphere of particle 2 (the spherical region of radius σ that surrounds a particle and cannot contain another particle center) completely masks the cavity. No other particle center besides 2 may make contact with the surface of the cavity. Hence, the conditional probability of observing a particle at R is governed solely by the particle-particle (1,2) correlation rather than the cavity-particle-particle ($g^{[3]}$) correlation. Using this information, one can exactly say for $\lambda \leqslant \sigma/2$ that $g^{[3]}(\lambda,\theta_2,R)=g(s)$, where $g(s)$ is the value of the pair correlation function for particles 1 and 2 separated by a distance s.

Due to the hard core interaction between particles 1 and 2, $g(s)$ is identically zero for $s<\sigma$. If we now choose a fixed value of R, s will take on its maximum value when the cavity and both particle centers are colinear, i.e., $s=R+\lambda$. Therefore, when $R+\lambda<\sigma$, s is always less than σ so that $g^{[3]}(\lambda,\theta_2,R)=0$. In this case, Eq. (13) reduces to

$$\frac{\partial \ln g(\lambda,R)}{\partial \lambda} = 4\pi\rho\lambda^2 G(\lambda), \quad \lambda \leqslant \frac{\sigma}{2}, \quad \lambda \leqslant R < \sigma - \lambda, \tag{14}$$

where the bound on R is modified as a reminder that $R \geqslant \lambda$. The initial condition necessary for solving Eq. (14) is $g(0,R)=1$, since no cavity-particle correlation exists when $\lambda=0$. By integrating and applying the initial condition we obtain [5]

$$g(\lambda,R) = \exp\left(4\pi\rho\int_0^\lambda G(r)r^2 dr\right) = \frac{1}{1-\frac{4}{3}\pi\rho\lambda^3},$$

$$\lambda \leqslant \frac{\sigma}{2}, \quad \lambda \leqslant R < \sigma - \lambda, \tag{15}$$

where the known form of $G(r)$ for $r \leqslant \sigma/2$ has been substituted [2]. It is interesting to see that in this subspace $g(\lambda,R)$ is not a function of R and is identical to $G(\lambda)$ [2].

III. SPT INTEGRAL EQUATION FOR THE CONFINED HARD SPHERE FLUID: CAVITY INTERSECTING A HARD WALL

In this section, the bulk fluid SPT integral equation is modified to describe the local density of hard spheres about a cavity that is intersecting a hard wall. Figure 3 defines the system geometry for the fluid confined by hard walls at one particular limit in the z direction, where the x and y directions are unconfined. The z coordinate originates a distance of $\sigma/2$ from the actual hard wall; $z=0$ is an effective hard wall to the particle centers because the particle centers may not approach the wall closer than $\sigma/2$. As discussed in our previous paper [1], the local density of hard sphere centers (when no cavity is present) is only a function of z, denoted by $\rho(z)$. As shown in Fig. 3, h is the z coordinate of the cavity center. For $h=0$, the portion of the cavity that extends beyond $z=0$ is hemispherical, while for $h<0$, the portion of the cavity beyond $z=0$ is shaped as a spherical cap (in which $\lambda \geqslant -h$). We do not consider cases for $h>0$ in this paper. Unlike a spherical cavity within a bulk fluid, the extension of SPT to this inhomogeneous system requires the use of a curvilinear coordinate system. With the center of the cavity at $z=h$ chosen as the origin, the vector coordinates for $\mathbf{r}$ are the length r and the angles θ and ϕ. θ is measured from a line perpendicular to $z=0$. ϕ is the rotation around this line. The coordinates may be easily changed from (r,θ,h) to z by the relationship $z=r\cos\theta+h$.

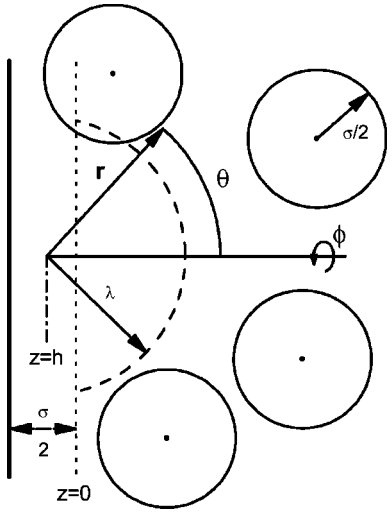

FIG. 3. An illustration of the chosen curvilinear coordinate system. λ is the radius of the cavity centered at $z=h \leqslant 0$. $\mathbf{r}$ is a vector originating from the cavity center and is described by the length r and the angles θ and ϕ. The origin of the z axis is located $\sigma/2$ from the hard wall where σ is the diameter of a hard particle. Only the portion of the cavity that extends to the right of $z=0$ is shown in which $\lambda \geqslant -h$.

A. General integral equation

Just like the bulk fluid, we begin by considering the following nearest neighbor distribution function. Consider an arbitrary point with z coordinate $h<0$ and suppose that a cavity of radius λ is centered at that point. We now denote the nearest neighbor distribution function by $\beta(\lambda,\mathbf{R},h)$ such that $\beta(\lambda,\mathbf{R},h)d\mathbf{R}$ is the probability of observing the nearest neighbor to the cavity at the vector position $\mathbf{R}$ within the volume element $d\mathbf{R}$ (noting that $|\mathbf{R}| \geqslant \lambda$). As before, this probability is also given by

$$\beta(\lambda,\mathbf{R},h)d\mathbf{R} = P_0(|\mathbf{R}|,h|\lambda,h)\rho G(\mathbf{R},h)d\mathbf{R}, \tag{16}$$

where $P_0(R,h|\lambda,h)$ is the probability that a cavity of radius $|\mathbf{R}|=R$ exists at $z=h$ on the condition that a cavity of radius

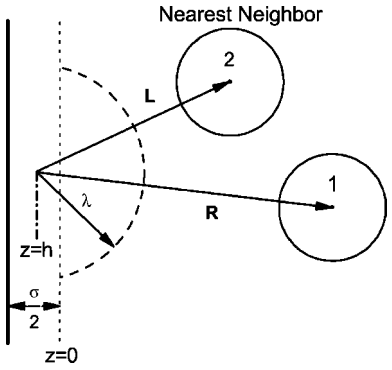

FIG. 4. Two-dimensional representation of a particular configuration of hard particles surrounding a cavity (shown by the long dashed line) of radius λ. The cavity is centered at $z=h\leqslant 0$. The main particle of interest is labeled as particle 1 and its vector position is given by **R**. The particle that is the nearest neighbor to the cavity is labeled as particle 2 and its position is given by **L**.

λ is already centered at $z=h$ and $\rho G(\mathbf{R},h)d\mathbf{R}$ is the probability that a particle center is found at **R** in $d\mathbf{R}$ on the surface of the cavity. Both $\beta(\lambda,\mathbf{R},h)$ and $G(\mathbf{R},h)$ are implicitly symmetric in ϕ; thus $\beta(\lambda,\mathbf{R},h)=\beta(\lambda,R,\theta,h)$ and $G(\mathbf{R},h)=G(R,\theta,h)$. Note that $R>-h$, otherwise the vector position **R** would not identify a relevant z. By argument of conditional probabilities,

$$P_0(R,h|\lambda,h)=\frac{P_0(R,h)}{P_0(\lambda,h)}=\exp\left(-2\pi\rho\int_\lambda^R \overline{G}(r,h)(r^2+rh)dr\right), \tag{17}$$

where we have introduced the I-SPT function $\overline{G}(\lambda,h)$ using Eq. (5). Entering the above into Eq. (16), we find that

$$\beta(\lambda,h,\mathbf{R})=\rho G(R,\theta,h)\exp\left(-2\pi\rho\int_\lambda^R \overline{G}(r,h)(r^2+rh)dr\right). \tag{18}$$

Again, the derivative of $\beta(\lambda,h,\mathbf{R})$ with respect to λ proves useful. Differentiation of Eq. (18) yields

$$\begin{aligned}\frac{\partial\beta(\lambda,h,\mathbf{R})}{\partial\lambda}&=\rho G(R,\theta,h)\exp\left(-2\pi\rho\int_\lambda^R \overline{G}(r,h)(r^2+rh)dr\right)\\&\quad\times[2\pi\rho\overline{G}(\lambda,h)(\lambda^2+\lambda h)]\\&=2\pi(\lambda^2+\lambda h)\rho\overline{G}(\lambda,h)\beta(\lambda,h,\mathbf{R}),\end{aligned} \tag{19}$$

where the second equality follows from substitution of Eq. (18).

Analogous to Sec. II, we now introduce the cavity-particle correlation function, $g(\lambda,h,\mathbf{R})$, where $\rho g(\lambda,h,\mathbf{R})d\mathbf{R}$ is the probability of finding a particle coordinate at **R** in $d\mathbf{R}$ on the condition that a cavity of radius λ is at $z=h$. Note that for $|\mathbf{R}|=\lambda$, when the particle is at the cavity surface, $g(\lambda,h,R,\theta)=G(\lambda,\theta,h)$. This conditional probability is dependent on whether the particle located at **R** (denoted by 1 in Fig. 4) is the nearest neighbor to the cavity or another particle (denoted by 2 in Fig. 4) is the nearest neighbor. Similar to Eq. (11), one can write the formally *exact* integral equation

$$\begin{aligned}\rho g(\lambda,h,\mathbf{R})d\mathbf{R}&=\beta(\lambda,h,\mathbf{R})d\mathbf{R}+\left(\int_{|\mathbf{L}|=\lambda}^{|\mathbf{L}|=R}\beta(\lambda,h,\mathbf{L})\rho\right.\\&\quad\left.\times g^{[3]}(\mathbf{L},\mathbf{R})d\mathbf{L}\right)d\mathbf{R},\end{aligned} \tag{20}$$

where $\rho g^{[3]}(\mathbf{L},\mathbf{R})d\mathbf{R}$ is the conditional probability of finding a particle at **R** in $d\mathbf{R}$, provided that a cavity of radius λ exists at $z=h$ and its nearest neighbor is at **L** in $d\mathbf{L}$. Again, the definition of $g^{[3]}$ is not tied to Eq. (20), and can be determined independently of Eq. (20) by either physical arguments or molecular simulation. The second term in Eq. (20) is integrated over all positions for which particle 2 is the nearest neighbor, i.e., $\lambda\leqslant|\mathbf{L}|\leqslant R$. Note that $\rho g(-h,h,\mathbf{R})=\rho(R\cos\theta+h)$, because for $\lambda=-h$ no portion of the cavity extends beyond $z=0$ so that $\rho g(-h,h,\mathbf{R})$ is simply the density of particles at the z coordinate corresponding to the vector position **R**. This same limit also applies for $R\gg\lambda$ where the influence of the cavity is no longer felt.

To obtain an expression for $g(\lambda,h,\mathbf{R})$ independent of $\beta(\lambda,h,\mathbf{R})$, we continue by differentiating Eq. (20) with respect to λ. After expanding $d\mathbf{L}$ in terms of the curvilinear coordinates (L,θ_2,ϕ_2) for particle 2, the result is

$$\begin{aligned}\rho\frac{\partial g(\lambda,h,\mathbf{R})}{\partial\lambda}&=\frac{\partial\beta(\lambda,h,\mathbf{R})}{\partial\lambda}-\rho\left(\lambda^2\int_0^{\cos^{-1}(-h/\lambda)}\sin\theta_2 d\theta_2\beta(\lambda,h,\lambda,\theta_2)\int_0^{2\pi}d\phi_2 g^{[3]}(\lambda,\theta_2,\phi_2,\mathbf{R})\right.\\&\quad\left.-\int_\lambda^R L^2dL\int_0^{\cos^{-1}(-h/L)}\sin\theta_2 d\theta_2\frac{\partial\beta(\lambda,h,L,\theta_2)}{\partial\lambda}\int_0^{2\pi}d\phi_2 g^{[3]}(L,\theta_2,\phi_2,\mathbf{R})\right).\end{aligned} \tag{21}$$

This equation is simplified by recognizing that $\beta(\lambda,h,\lambda,\theta_2)=\rho G(\lambda,\theta_2,h)$, which is the local density at θ_2 on the surface of the cavity. Substituting Eq. (19) into the above yields, upon rearrangement,

$$\frac{\partial g(\lambda,h,\mathbf{R})}{\partial\lambda}=2\pi(\lambda^2+\lambda h)\rho\overline{G}(\lambda,h)g(\lambda,h,\mathbf{R})-\rho\lambda^2\int_0^{\cos^{-1}(-h/\lambda)}\sin\theta_2 d\theta_2 G(\lambda,h,\theta_2)\int_0^{2\pi}d\phi_2 g^{[3]}(\lambda,\theta_2,\phi_2,\mathbf{R}). \tag{22}$$

Although the ϕ_2 dependence remains in $g^{[3]}$ because the fluid is not isotropic, the resulting integral equation for $g(\lambda,h,\mathbf{R})$ is analogous to the expression derived by Reiss *et al.* [5,7] for bulk cavities. Since $g^{[3]}$ is not known in general, further manipulation of the integral equation relies upon the generation of closure conditions for $g^{[3]}$. By closely examining Eq. (22), we again see that $L=\lambda$ in $g^{[3]}$, meaning that $g^{[3]}$ needs to be evaluated when the center of particle 2 resides on the cavity surface. Similar to the bulk SPT integral equation, we can use this restriction to provide an exact closure condition and, hence, an exact solution of Eq. (22).

B. Exact closure of $g^{[3]}(\lambda,\theta_2,\phi_2,\mathbf{R})$

Since $g^{[3]}$ is evaluated for $L=\lambda$, the only configurations of interest are similar to the one depicted in Fig. 5. For this configuration, we choose $\lambda \leqslant \sqrt{h^2+(\sigma/2)^2}$, which causes the exclusion sphere of particle 2 to completely mask the cavity. In this case, the cavity does not contribute to the three-body correlation. Only the particle-particle correlation matters. Furthermore, particle-particle (1, 2) interactions are not allowed for particle separation distances of s less than σ since the hard cores of each particle prevent such overlaps from occurring. Thus, for all configurations in which $s<\sigma$, $g^{[3]}(\lambda,\theta_2,\phi_2,\mathbf{R})$ is identically zero. Unfortunately, this requirement is fulfilled by a large number of radius-position combinations, and the resulting subspace is not easily described. There is, however, a bound on R below which all combinations lie in this subspace. This bound on R is found when the cavity and both particle centers are colinear along the $z=0$ plane, i.e., $s=\sqrt{\lambda^2-h^2}+\sqrt{R^2-h^2}$ (particle 2 resides above the cavity and particle 1 is below the cavity). Since $R \geqslant \lambda$ and we are considering configurations in which $s<\sigma$, the restriction on R for this formally *exact* region becomes $\lambda \leqslant R < \sqrt{\sigma^2-2\sigma\sqrt{\lambda^2-h^2}+\lambda^2}$. With this restriction, the integral equation reduces to

$$\frac{\partial \ln g(\lambda,h,\mathbf{R})}{\partial\lambda} = 2\pi(\lambda^2+\lambda h)\rho\overline{G}(\lambda,h),$$

$$-h<\lambda \leqslant \sqrt{h^2+\left(\frac{\sigma}{2}\right)^2}, \quad s<\sigma. \tag{23}$$

Finally, integration from $-h$ to λ yields

$$g(\lambda,h,\mathbf{R}) = \frac{\rho(R\cos\theta+h)}{\rho} \times \exp\left(2\pi\rho\int_{-h}^{\lambda}\overline{G}(r,h)(r^2+rh)dr\right),$$

$$-h<\lambda \leqslant \sqrt{h^2+\left(\frac{\sigma}{2}\right)^2}, \quad s<\sigma, \tag{24}$$

where the initial condition $\rho(R\cos\theta+h)/\rho$ has been entered for $g(-h,h,\mathbf{R})$. This expression for the cavity-particle correlation function can be simplified by recognizing that the exponential term is equal to $1/P_0(\lambda,h)$ [see Eq. (5)] resulting in

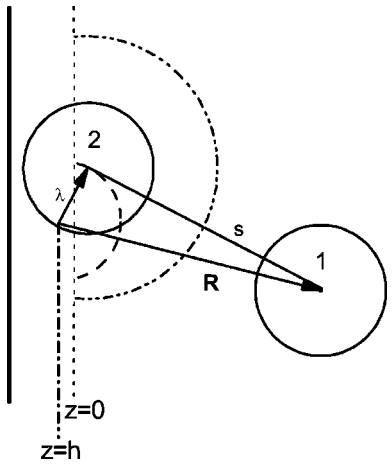

FIG. 5. The two-dimensional representation of a relevant configuration for $g^{[3]}(\lambda,\theta_2,\phi_2,\mathbf{R})$. The long dashed line represents the cavity of radius λ centered at $z=h\leqslant 0$, in this case $\lambda \leqslant \sqrt{h^2+(\sigma/2)^2}$. Particle 2, the nearest neighbor, is located on the surface of the cavity as demanded by $g^{[3]}(\lambda,\theta_2,\phi_2,\mathbf{R})$. R is the distance from the cavity center to particle 1 and s is the distance between the particle centers. The dashed-dot line represents the exclusion sphere of particle 2.

$$g(\lambda,h,R,\theta) = \frac{\rho(R\cos\theta+h)}{\rho}\frac{1}{P_0(\lambda,h)},$$

$$-h<\lambda \leqslant \sqrt{h^2+\left(\frac{\sigma}{2}\right)^2}, \quad s<\sigma, \tag{25}$$

where we have eliminated the vector notation.

Equation (25) can be used to generate exact information about the local density at the cavity surface, or the I-SPT function $G(\lambda,\theta,h)$. As noted before, when $R=\lambda$, $g(\lambda,h,\lambda,\theta)=G(\lambda,\theta,h)$. Therefore, $G(\lambda,\theta,h)$ for this λ-range is given *exactly* by

$$G(\lambda,\theta,h) = \frac{\rho(\lambda\cos\theta+h)}{\rho}\frac{1}{P_0(\lambda,h)} = \frac{\rho(\lambda\cos\theta+h)}{\rho\left(1-\pi\int_0^{\lambda+h}\rho(z)[\lambda^2-(z-h)^2]dz\right)},$$

$$-h \leqslant \lambda \leqslant \sqrt{h^2+\left(\frac{\sigma}{2}\right)^2}, \tag{26}$$

where the second equality results from the substitution of the exact form of $P_0(\lambda,h)$ given in Eq. (3). If the second line of Eq. (26) is averaged over $0\leqslant\theta\leqslant\cos^{-1}(-h/\lambda)$, followed by a change of variables from (λ,θ) to z, $\overline{G}(\lambda,h)$ as shown in Eq. (4) is recovered, thereby demonstrating consistency with I-SPT [1].

A closer examination of Eq. (26) provides the additional derived information regarding the function $G(\lambda,\theta,h)$. At least for $z\leqslant\sigma/2$, the density profile $\rho(z)$ decreases with an increase in z. Therefore, $G(\lambda,\theta,h)$ is an increasing function

of θ for fixed λ and h. This trend is expected to continue for cavity radii that fall outside the exact range. A particularly interesting result is obtained for $\theta_c=\cos^{-1}(-h/\lambda)$, the interface of the "three phases" (cavity-wall-fluid) where the cavity surface intersects the $z=0$ plane. Entering θ_c into Eq. (26) yields

$$G(\lambda,\theta_c,h)=\frac{\rho(0)}{\rho}\frac{1}{P_0(\lambda,h)}=\frac{p}{\rho kT}\frac{1}{P_0(\lambda,h)},$$

$$\lambda\leqslant\sqrt{h^2+\left(\frac{\sigma}{2}\right)^2}. \tag{27}$$

Since $P_0(\lambda,h)\leqslant 1$, $G(\lambda,\theta_c,h)\geqslant p/\rho kT$ for radii in this range. In other words, the local density at the three-phase interface is enhanced above the hard wall contact value of p/kT.

While this density enhancement can be explained using physical arguments (as will be done later), it is seemingly at odds with the initial *decrease* in $\overline{G}(\lambda,h)$ with an increase in λ reported in Ref. [1]. Because the density at the three-phase interface exceeds p/kT, the density around the remaining portion of the cavity must therefore be less, perhaps significantly, than p/kT so that the average density at the cavity surface is always less than p/kT. In fact, this can be inferred analytically for cavities in the exact range. The ratio between the local density at the cavity surface at $\theta=0$ and $\theta=\theta_c$ is given by

$$\frac{\rho G(\lambda,0,h)}{\rho G(\lambda,\theta_c,h)}=\frac{\rho(\lambda+h)}{\rho(0)}. \tag{28}$$

Since simulation-generated density profiles indicate that $\rho(z)$ is always less than $\rho(0)=p/kT$ for $z>0$, the ratio in Eq. (28) is always less than unity. Consequently, for cavities in the exact range ($\lambda\leqslant\sqrt{h^2+(\sigma/2)^2}$), the local density at the front of the cavity is less than that at the three-phase interface. [This result is true in general since $\overline{G}(\lambda,h)\leqslant p/\rho kT$ and, as observed via molecular simulation, a density enhancement above p/kT always appears at the three-phase interface for larger radii.] A detailed discussion of how the above-mentioned properties of $G(\lambda,\theta,h)$ give rise to a minimum in $\overline{G}(\lambda,h)$ is delayed to the following section.

Since the hemispherical cavity ($h=0$) was shown to be a special case in that the minimum of its average I-SPT function, $\overline{G}(\lambda)$, was always found in the exact λ-range ($\lambda\leqslant\sigma/2$) [1], we now present some equations applicable to this system. For ease of notation we drop the h dependence, so that $g(\lambda,h=0,R,\theta)\equiv g(\lambda,R,\theta)$. Hence, entering $h=0$ into Eq. (24) yields the formally *exact* relation

$$g(\lambda,R,\theta)=\frac{\rho(R\cos\theta)}{\rho}\exp\left(2\pi\rho\int_0^\lambda\overline{G}(r)r^2dr\right)$$

$$=\frac{\rho(R\cos\theta)}{\rho}\frac{1}{P_0(\lambda)},\quad \lambda\leqslant\frac{\sigma}{2},\quad \lambda\leqslant R<\sigma-\lambda. \tag{29}$$

$G(\lambda,\theta)$ for $h=0$ is recovered by evaluating Eq. (29) at $R=\lambda$ and substituting the exact form of $P_0(\lambda)$ to yield

$$G(\lambda,\theta)=\frac{\rho(\lambda\cos\theta)}{\rho\left(1-\pi\int_0^\lambda\rho(z)(\lambda^2-z^2)dz\right)},\quad \lambda\leqslant\frac{\sigma}{2}. \tag{30}$$

Evaluating the above at $\theta=\pi/2$, where the cavity overlaps the hard wall, again reveals an enhancement of the local density above the hard wall contact value of p/kT. This *exact* form of $G(\lambda,\theta)$ will be used in the next section to explain why the minimum of $\overline{G}(\lambda)$ occurs before $\sigma/2$, despite $G(\lambda,\pi/2)\geqslant p/\rho kT$.

IV. RESULTS

In what follows, we examine the cavity-particle correlation function as generated via the exact formulas and Monte Carlo (MC) simulation. The density profiles may be generated for any of the geometries described in the previous section ($h\leqslant 0$), but we show results for hemispherical cavities only. The conclusions drawn for the hemispherical cavity will apply to the other cases as well.

We performed MC simulations in the isothermal-isobaric (NpT) ensemble with hard walls imposed at the z-limits and periodic boundary conditions in the x and y Cartesian directions [9,10]. The position of the cavity center located at $z=h\leqslant 0$ and its radius λ were fixed for the duration of the simulation. Five hundred hard particles were used to ensure the existence of a bulk phase in the middle of the simulation cell. After a equilibration/relaxation period of 3×10^4 cycles (N particle moves and one volume adjustment per cycle), the simulation began the production run of accumulating the appropriate averages. During the production run, the simulation sampled for $g(\lambda,h,\mathbf{R})$ by measuring the density profile surrounding randomly placed cavities every five cycles. The x and y positions of the cavity centers were chosen at random, while the z-position was fixed at $z=h$ relative to one of the walls (the particular wall was also selected at random). If a cavity was successfully inserted at this location (i.e., no particle centers were found inside the cavity), a counter was updated and the density profile surrounding the cavity was then sampled by measuring the radial distance R and angle θ to each particle center in the simulation cell. After N trial insertions the simulation resumed normal MC moves. Density profiles were sampled after every 5 MC cycles with a total simulation length of 10^6 production cycles being performed. Afterward, the average density at each (R,θ) position was normalized to yield the function $g(\lambda,h,R,\theta)$. This method provides better sampling of the density profile around the cavity compared to generating density profiles about a small number of cavities that are always maintained inside the simulation cell. Unfortunately, this method becomes inefficient for large cavity radii and higher bulk densities because the probability of randomly observing large cavities is extremely low. Finally, the details of how $\rho(z)$ was generated during the simulation are found in Ref. [1].

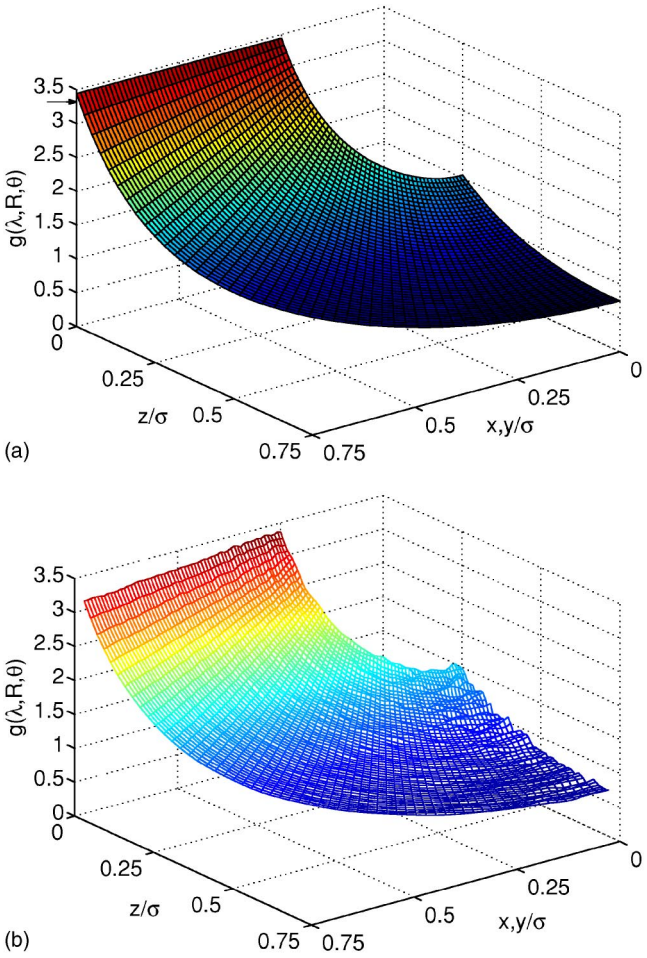

FIG. 6. (Color online) (a) $g(\lambda,R,\theta)$ calculated from simulation-generated $\rho(z)$ for $\lambda=\sigma/4$ and $\rho\sigma^3=0.5$. The hard wall contact value of $p/\rho kT=3.3070$ is indicated by the arrow. z is the distance from the effective hard wall and is related to (R,θ) by $z=R\cos\theta$. x and y represent normal distances to the cavity center. $g(\lambda,R,\theta)$ exceeds $p/\rho kT$ for $\theta=\pi/2$, corresponding to $z=0$ ($\theta=0$ corresponds to $x,y=0$). For fixed z, $g(\lambda,R,\theta)$ is constant. (b) $g(\lambda,R,\theta)$ generated via MC simulation for $\lambda=\sigma/4$ and $\rho\sigma^3=0.5$. The simulation-generated $g(\lambda,R,\theta)$ is nearly identical to the exact result, showing enhancement beyond $p/\rho kT$ for $\theta=\pi/2$ and constant $g(\lambda,R,\theta)$ for fixed z.

A. Exact $g(\lambda,R)$: Hemispherical cavity

Figure 6(a) displays the exact $g(\lambda,R,\theta)$ for a hemispherical cavity ($h=0$) of $\lambda=\sigma/4$ in the range of $R\leqslant 3\sigma/4$ and for a bulk density of $\rho\sigma^3=0.5$. For this cavity radius and bulk density $P_0(\lambda)=0.9597$ as calculated from $\overline{G}(\lambda)$ [1]. We also observe that $g(\lambda,R,\pi/2)=3.446$ (for positions corresponding to $z=0$), which exceeds the hard wall contact value of $p/\rho kT=3.307$. In addition, Fig. 6(a) reveals that $g(\lambda,R,\theta)$ is constant for a fixed z and that $g(\lambda,R,\theta)$ decreases with an increase in z, results which are both predicted by Eq. (29). In fact, $g(\lambda,R,\theta)$ decreases below unity for positions near $\theta=0$ (corresponding to $x,y=0$ in the figure), indicating that the density of particle centers near the front of the cavity is depleted below that of the bulk density. This behavior of

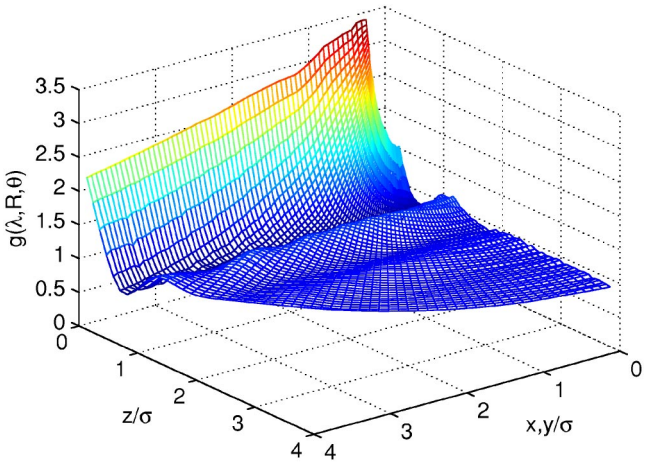

FIG. 7. (Color online) $g(\lambda,R,\theta)$ generated via MC simulation for $\lambda=\sigma/4$ and $\rho\sigma^3=0.5$. z is the distance from the effective hard wall, while x and y represent the respective distance from the cavity center. The local density is enhanced beyond p/kT for $z=0$ and for small x or y. For positions far from the cavity center, $g(\lambda,R,\theta)$ resembles the wall-fluid density profile $\rho(z)$. The apparent decrease in $g(\lambda,R,\theta)$ along $z=0$ is not a true decrease, but is a result of the method used to count particle centers in a solid angle wedge.

$g(\lambda,R,\theta)$ is common to radii in the exact range ($\lambda\leqslant\sigma/2$) for any fluid density. We also present in Fig. 6(b) the corresponding simulation-generated $g(\lambda,R,\theta)$. The simulation results are nearly identical to the exact $g(\lambda,R,\theta)$. An enhancement in the local density above $p/\rho kT$ is seen for $z=0$, $g(\lambda,R,\theta)$ is constant for fixed z, and $g(\lambda,R,\theta)$ decreases as z increases.

In both plots of Fig. 6, the cause of the initial decrease in $\overline{G}(\lambda)$ with an increase in λ becomes apparent. As anticipated by the analytical expressions for $G(\lambda,R,\theta)$, the local density at the front ($\theta=0$) of the cavity is less than that at the three-phase interface ($\theta=\pi/2$). The local density around most of the cavity, however, is sufficiently lower than the $\lambda=0$ limit of $\rho\overline{G}(0)=p/kT$, thereby causing the average density to fall below p/kT. As the radius of the hemispherical cavity initially increases, the cavity "sees" a rapidly decreasing local density at the front of cavity. The net effect is a reduction of the average density surrounding the cavity.

B. Simulation $g(\lambda,R)$: Hemispherical cavity

We also used molecular simulation to investigate $g(\lambda,R,\theta)$ for cavity radii, as well as values of R, outside the exact range. Figure 7 extends the range of the results in Fig. 6(b) beyond the exact limit of $R=3\sigma/4$ for $\lambda=\sigma/4$ and $\rho\sigma^3=0.5$. Although the density of particle centers is enhanced in the region immediately surrounding the cavity, the density perturbation caused by the cavity does not extend that far into the fluid. For distances in the z direction greater than about 1.5σ from the cavity center, the distribution of particles resumes its normal shape, becoming nearly identical to $\rho(z)$. The apparent decrease in $g(\lambda,R,\theta)$ along $z=0$ in Fig. 7 is an artifact of the method used to determine g, not an actual decrease. Particle centers are counted in solid angle

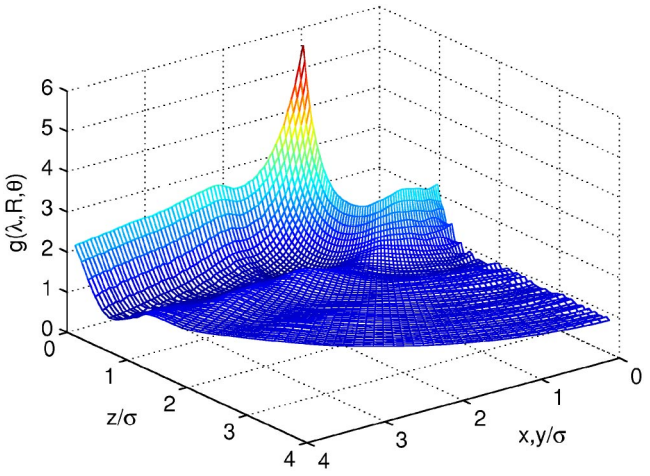

FIG. 8. (Color online) $g(\lambda,R,\theta)$ for $\lambda=\sigma$ and $\rho\sigma^3=0.5$ generated via MC simulation. z is the distance from the effective hard wall and x and y measure the perpendicular distances from the cavity center. The density is enhanced beyond $p/\rho kT$ at the three-phase interface, but the enhancement is localized close to $x=y=\sigma$ and $z=0$. Far from the cavity center, $g(\lambda,R,\theta)$ resembles $\rho(z)$. Along $\theta=0$, however, $g(\lambda,R,\theta)$ resembles the bulk RDF $g(R)$.

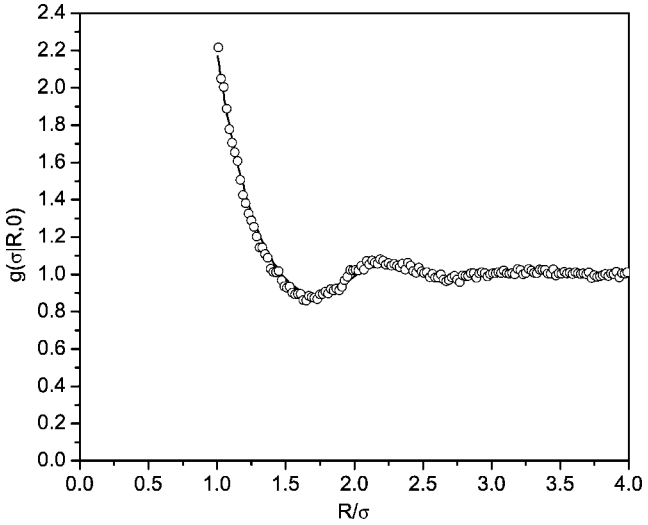

FIG. 9. The cavity-particle function $g(\sigma,R,0)$ and bulk RDF $g(R)$ plotted versus radial distance R for $\rho\sigma^3=0.5$. $g(R)$ is denoted by the solid line and $g(\sigma,R,0)$ by the circles. A cavity of radius $\lambda=\sigma$ is equivalent to a particle of diameter σ [2]. The two functions are nearly identical and deviations may be attributed to simulation noise.

wedges that become larger with increasing R, artificially decreasing g for large R and θ near $\pi/2$. Far from the cavity center, the correct value of g for $\theta=\pi/2$ $(z=0)$ is $p/\rho kT$.

The shape of $g(\lambda,R,\theta)$, however, is quite different at larger cavity radii. Figure 8 shows $g(\lambda,R,\theta)$ for $\lambda=\sigma$ and $\rho\sigma^3=0.5$ as generated by MC simulation. [Again, the previously mentioned artificial decrease appears along $z=0$, due to the method chosen to count particles at various (R,θ) pairs.] Note that this cavity is equivalent to a hard sphere placed at $z=0$. In this case, $g(\lambda,R,\theta)$ at $R=\lambda$ and $\theta=\pi/2$ is enhanced to 5.588, exceeding the corresponding values for cavities of $\lambda\leqslant\sigma/2$ [e.g., for $\rho\sigma^3=0.5$ and $\lambda=\sigma/2$, $g(\lambda,R,\theta)$ at $R=\lambda$ and $\theta=\pi/2$ equals 3.512]. Yet, the enhancement at the three-phase contact rapidly decays with θ; the density increase is concentrated within a narrow region in contrast to the broad enhancement observed for small cavities. We also see that the first minimum of the density profile nearly wraps around the cavity, forming a distinct trough in $g(\lambda,R,\theta)$. The location of this minimum is commensurate with the first minimum of the wall-fluid density profile $\rho(z)$ for positions near $\theta=\pi/2$ or far from the cavity, but resembles the bulk radial distribution function (RDF), $g(R)$, for positions near $\theta=0$. In Fig. 9, both $g(\lambda,R,\theta)$ for $\lambda=\sigma$ and $\theta=0$ and the bulk RDF, obtained from a separate bulk fluid MC simulation, are shown for $\rho\sigma^3=0.5$. The two correlation functions are nearly identical, suggesting that particles near $\theta=0$ interact with the cavity without regard to the wall, i.e., the particles in front of the cavity are unable to "sense" the wall. For intermediate values of θ, $g(\lambda,R,\theta)$ transitions between $g(R)$ and $\rho(z)$. Trends similar to those seen in Figs. 7 and 8 are also observed for $h<0$.

The density enhancement exhibited by $g(\lambda,R,\theta)$ near the three-phase interface is an interesting conclusion of our integral equation and simulation studies. This enhancement is not, however, entirely unexpected as similar behavior was reported by Henderson in a study of hard spheres adsorbed in wedges [11]. Since hard particles are most likely to reside in locations that are protected from collisions with other particles, particles therefore congregate near a given boundary. For the cavity geometries studied here, a particle is most shielded from interactions with other particles when it is located at the intersection of the cavity with the hard wall. A particle at this position will experience collisions only from the "fluid" side of the particle; no collisions will occur on the cavity side. Thus, an effective force develops that serves to push the particle towards the three-phase interface. This effective force is strongest around the point where the cavity intersects the hard wall, so that the density enhancement is largest in the three-phase interfacial region. Moreover, and particularly for small λ, this enhancement will deplete the number of particles that reside near the remaining portion of the cavity surface. The exclusion sphere of a particle located at the three-phase interface overlaps the majority of the cavity surface (or completely covers the cavity when $\lambda\leqslant\sigma/2$), thereby lowering the probability, and so local density, of finding a particle away from $z=0$.

The comparison of Fig. 8 with Fig. 6 also reveals why $\overline{G}(\lambda)$ begins to increase again for large enough λ. The average density along the cavity surface for $\lambda=\sigma$ clearly exceeds the average density for $\lambda=\sigma/4$, i.e., $\overline{G}(\sigma)>\overline{G}(\sigma/4)$. So while Fig. 6 shows that $\overline{G}(\lambda)$ initially decreases, Fig. 8 indicates that $\overline{G}(\lambda)$ begins to increase at a large enough cavity radius. Consequently, $\overline{G}(\lambda)$ exhibits a minimum at some intermediate cavity radius.

Figure 8 also validates the limiting condition of $\overline{G}(\lambda)$ for $\lambda\to\infty$ used in Ref. [1]. In Fig. 8, $g(\lambda,R,\theta)=g(\lambda,R)$ (the bulk cavity-particle correlation function) around $\theta=0$. So, along this portion of the cavity surface, $g(\lambda=R)=G(\lambda)$,

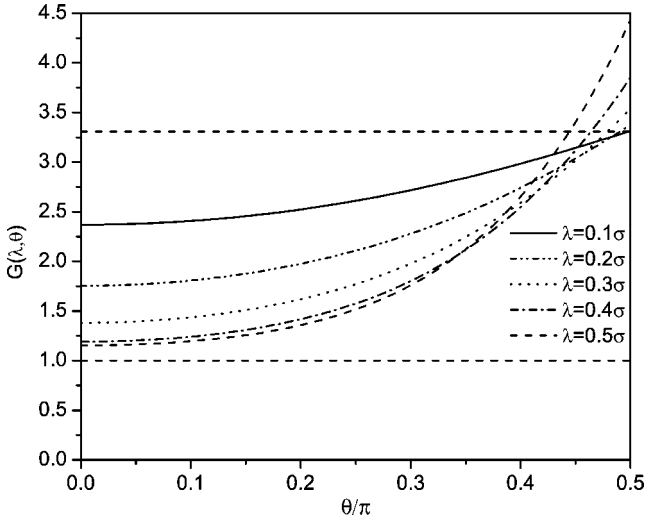

FIG. 10. $G(\lambda,\theta)$ versus θ/π for $\rho\sigma^3=0.5$ and various cavity radii. λ is the cavity radius and θ measures the angle from the z axis. The upper horizontal dashed line denotes $G(\lambda=0,\theta)=p/\rho kT=3.30704$. The density enhancement at $\theta/\pi=1/2$ (or $\theta=\pi/2$) increases with λ, while the density decreases with λ at $\theta=0$.

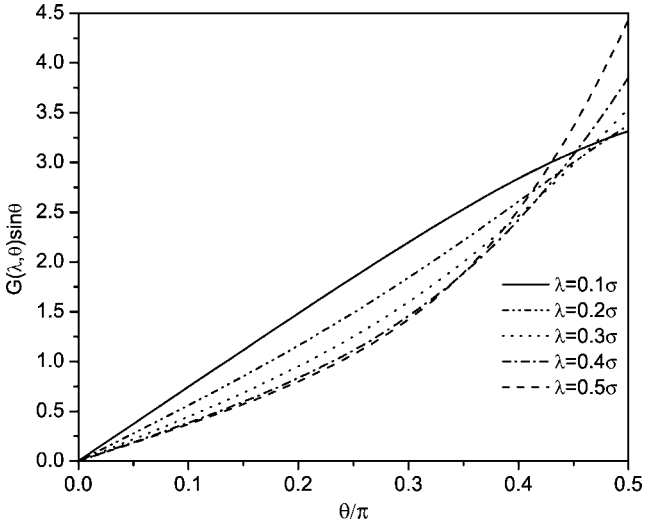

FIG. 11. $G(\lambda,\theta)\sin\theta$ versus θ/π for $\rho\sigma^3=0.5$ and various cavity radii. λ is the cavity radius and θ measures the angle from the z axis. $G(\lambda,\theta)$ is multiplied by $\sin\theta$ to show the term that is integrated to obtain $\overline{G}(\lambda)$. In this figure, $\overline{G}(\lambda)$ is equivalent to the area under the curve.

where $G(\lambda)$ is the bulk SPT cavity function. For larger λ, the local density of particle centers at the cavity surface will still equal the bulk $G(\lambda)$, but for an even larger range of θ about $\theta=0$. Thus, as $\lambda\to\infty$, the average density at the cavity surface should approach $G(\infty)$, thereby confirming the limit that $\overline{G}(\infty)=G(\infty)=p/\rho kT$. In addition, since the density around $\theta=\pi/2$ is greater than p/kT, the average density at the cavity surface exceeds $G(\lambda)$. This explains the trend seen in Ref. [1] in which $\overline{G}(\lambda)\geqslant G(\lambda)$. The appearance of the density enhancement at $\theta=\pi/2$ also explains why $\overline{G}(\lambda)$ approaches its limiting value of $p/\rho kT$ much faster than $G(\lambda)$. Furthermore, the enhancement of the local density above p/kT at $\theta=\pi/2$ implies that $\overline{G}(\infty)$ goes to $p/\rho kT$ from above, and not from below as was observed in Ref. [1]. The corresponding density depletion away from, but still near, $\theta=\pi/2$, shows, however, why $\overline{G}(\infty)$ approaches $p/\rho kT$ from below.

C. Minimum in $\overline{G}(\lambda)$

Taken together, Figs. 6 and 8 provide an explanation as to why $\overline{G}$ exhibits a minimum. In light of Fig. 8, one might also expect that the minimum appears at a cavity radii close to $\lambda=\sigma$. Yet, in Ref. [1] the minimum in $\overline{G}(\lambda)$ always appeared for $\lambda\leqslant\sigma/2$, where the density profiles that develop around the cavities are similar to those shown in Figs. 6 and 7 (and not Fig. 8).

Since the minimum in $\overline{G}(\lambda)$ always falls within the exact range of $\lambda\leqslant\sigma/2$, the exact solution of the integral equation allows us to explore in greater detail the origin and location of the minimum. For example, $G(\lambda,\theta)$ at $\rho\sigma^3=0.5$, obtained using Eq. (30) and a simulation generated $\rho(z)$, is plotted versus θ/π in Fig. 10 for various cavity radii λ less than $\sigma/2$. As the cavity radius increases, two trends appear: the density at $\theta=\pi/2$ increases while the density at $\theta=0$ decreases. These trends show that the hard wall has different effects on $G(\lambda,\theta)$ depending on the value of θ. Regardless of λ, $G(\lambda,\theta)$ is greater than $p/\rho kT$ at $\theta=\pi/2$, indicating that the hard wall plays a large role in determining the fluid structure. The trend for $\theta=0$ is more complex. The decrease in $G(\lambda,\theta)$ for θ near zero seems to depend on how much fluid is displaced by the cavity and the portion of $\rho(z)$ the cavity "sees" upon insertion. For example, a cavity of radius $\lambda=0.1\sigma$ displaces a small amount of fluid. Hence, the fluid environment that surrounds the cavity is very similar to $\rho(z)$, leading to a $\overline{G}(\lambda)$ that is close in value to (though less than) $p/\rho kT$. For $\lambda=0.5\sigma$, however, more fluid is displaced and the resulting fluid environment yields a much reduced average density in contact with the cavity surface.

The cause of the initial decrease of $\overline{G}(\lambda)$ from $p/\rho kT$ is readily apparent in Fig. 10. While the density at $\pi/2$ increases with an increase in λ, the large decrease in the density along the majority of the cavity surface is sufficient to cause the *average* density to decrease. These two effects are in competition to determine whether $\overline{G}(\lambda)$ will increase or decrease with a change in λ. This competition is displayed more clearly in Fig. 11, where plots of $G(\lambda,\theta)$ multiplied by $\sin\theta$, the actual term that is integrated in Eq. (1) to obtain $\overline{G}(\lambda)$, are shown. In Fig. 11, the plots for each radii must necessarily begin at zero, further diminishing the contribution to $\overline{G}(\lambda)$ for small θ. Because $\overline{G}(\lambda)$ is defined as the integral of $G(\lambda,\theta)\sin\theta$, the area under each curve equals $\overline{G}(\lambda)$. One can see in Fig. 11 that the area under each curve decreases as λ approaches 0.4σ, but then increases as λ increases to 0.5σ. In other words, $\overline{G}(\lambda)$ has passed through a minimum, just as is observed in Fig. 4 of Ref. [1]. The actual minimum for this density occurs at $\lambda=0.405\sigma$ [1]. Closer examination of Figs. 10 and 11 shows that the increase in

$\overline{G}(\lambda)$ as λ increases from 0.4σ to 0.5σ is almost entirely due to the density enhancement near $\theta=\pi/2$. From $\theta=0$ to $\theta \approx \pi/3$, $G(\lambda,\theta)$ does not vary much in value as λ increases from 0.4σ to 0.5σ. Similar trends are also seen at other densities. Another interesting result of Fig. 11 is that the curvature of $G(\lambda,\theta)\sin\theta$ changes sign from negative to positive as λ increases from 0.1σ to 0.2σ. This seems to be due to the relatively small slope of $G(\lambda,\theta)$ for $\lambda=0.1\sigma$, which yields a negative curvature when multiplied by $\sin\theta$.

Although such plots of $G(\lambda,\theta)\sin\theta$ clearly indicate why $\overline{G}(\lambda)$ exhibits a minimum, these curves still do not reveal precisely why the minimum always occurs before $\lambda=\sigma/2$ for all fluid densities. This is an issue which remains to be resolved. A derivative of $G(\lambda,\theta)$ in Eq. (30) with respect to λ does not, unfortunately, prove to be particularly useful in understanding the behavior of $G(\lambda,\theta)\sin\theta$ since the properties of $\rho(z)$ are not known in general. Figure 10 reveals that $\partial G(\lambda,\theta)/\partial\lambda=0$ for all λ but only within a small range of θ near $\pi/2$. In turn, $\partial G(\lambda,\theta)/\partial\lambda=0$ is connected to the appearance of the minimum in $\overline{G}(\lambda)$ as seen in Fig. 11. But it is difficult to infer why $\partial G(\lambda,\theta)/\partial\lambda=0$ only for certain θ, since $\rho(z)$ is not known in general and varies considerably with the bulk density. One can show, however, that $\partial G(\lambda,\theta)/\partial\lambda=0$ does not coincide with the appearance of the first local minimum in $\rho(z)$.

The minimum in $\overline{G}(\lambda)$, which may also be interpreted as a decrease in the pressure on the cavity surface, also has ties to surface thermodynamics. The decrease in G can be connected to the appearance of the three-phase interface (cavity-wall-fluid) and its associated line tension. (In the hard disk fluid, it would be the *point* tension [12].) When a cavity grows in a uniform hard particle fluid, the local fluid pressure on its surface will increase. For cavities placed at a hard wall, however, another relation, the mechanical balance of forces at the three-phase interface, is required to fully describe the surface thermodynamics. This second relation allows either an increase or decrease in the local fluid pressure at the cavity surface depending on the sign of the line tension. Because inhomogeneous SPT predicts a decrease in $\overline{G}(\lambda)$, so that the local fluid pressure decreases as well, the corresponding line tension should be negative. At large enough cavity sizes, the pressure on the cavity surface will eventually exceed the contribution of the three-phase interfacial tension so that $\overline{G}(\lambda)$ must increase with an increase in λ.

V. CONCLUSION

We have presented a new SPT integral equation that describes the fluid structure surrounding cavities which overlap a hard, structureless wall. The equation is based on the ideas of scaled particle theory and is valid for the hard sphere fluid confined between planar hard walls. Derivation of the integral equation relies on the definition of an exact three-body correlation $g^{[3]}$, which is not known in general. Consideration of specific cavity sizes and positions, however, provides a closure condition on $g^{[3]}$ and, in turn, an exact solution of the integral equation. Plots of $g(\lambda,R,\theta)$ generated by the solution of the integral equation agree with simulation results within the range of the exact closure. The integral equation can also be easily extended to cavities within the two-dimensional hard disk fluid [13].

Solution of the integral equation shows that the density of particle centers is enhanced in the region where the cavity overlaps the effective hard wall. At small cavity sizes, this enhancement extends uniformly along the hard wall. Simulation results showed that the enhancement is localized at the three-phase interface for cavity radii outside the exact range ($\lambda \leqslant \sigma/2$). The density enhancement is also responsible at small cavity radii for reducing the density around the remaining portion of the cavity. The balance between these two competing effects (enhancement versus depletion) determines the behavior of the average density surrounding a cavity and ultimately explains why $G(\lambda)$ displays a minimum. Why the minimum always occurs for $\lambda<\sigma/2$, however, is still not clearly known.

As noted in the Introduction, insights into the various properties of $G(\lambda,\theta,h)$ have the potential to help explain various depletion phenomena of hard particle systems. The reported enhancement at the three-phase interface is likely to play a large role in determining whether the depletion force is attractive or repulsive since the large enhancement might counteract particles "pushing" the cavity (or equivalent solute) toward the wall. With the range over which the integral equation can be solved essentially limited to $\lambda \leqslant \sigma/2$, our analytical approach is so far restricted to small cavities, but the conclusions drawn here should shed light on depletion effects in general. In a forthcoming paper, the exact knowledge of $G(\lambda,\theta,h)$ is shown to be important in understanding the behavior exhibited by the normal force needed to "push" a cavity from behind the wall and into the fluid.

Overall, the present work provides a crucial first step in fully describing the fluid structure surrounding a cavity near a hard wall. Beyond the simple exact closure condition used here to solve the integral equation, there remains the opportunity to propose additional approximate closure conditions for the three-body correlation function to solve the integral equation for a larger range of λ and R. Also, the presented equations are valid only for cavity centers in which $h \leqslant 0$ and can be extended to account for $h>0$. A full treatment and solution of the integral equations should provide invaluable information regarding the structure of the confined hard sphere fluid and the behavior of hard spherelike colloidal dispersions.

ACKNOWLEDGMENT

This material is based upon work supported by the National Science Foundation under Grant No. 0133780.

[1] D. W. Siderius and D. S. Corti, preceding paper, Phys. Rev. E **71**, 036141 (2005).
[2] H. Reiss, H. L. Frisch, and J. L. Lebowitz, J. Chem. Phys. **31**, 369 (1959).
[3] E. Helfand, H. L. Frisch, and J. L. Lebowitz, J. Chem. Phys. **34**, 1037 (1961).
[4] R. Dickman, P. Attard, and V. Simonian, J. Chem. Phys. **107**, 205 (1997).
[5] H. Reiss and R. V. Casberg, J. Chem. Phys. **61**, 1107 (1974).
[6] L. P. Chua, M.S. thesis, Purdue University, West Lafayette, Indiana, 2002.
[7] H. Reiss, H. M. Ellerby, and J. A. Manzanares, J. Phys. Chem. **100**, 5970 (1996).
[8] M. D. Heying and D. S. Corti, J. Phys. Chem. B **108**, 19756 (2004).
[9] J. E. Finn and P. A. Monson, Mol. Phys. **65**, 1345 (1988).
[10] J. E. Finn and P. A. Monson, Langmuir **5**, 639 (1989).
[11] J. D. Henderson, J. Chem. Phys. **120**, 1535 (2004).
[12] A. I. Rusanov, Colloids Surf., A **159**, 315 (1999).
[13] D. W. Siderius, M.S. thesis, Purdue University, West Lafayette, Indiana, 2004.